*Materials Science and Engineering A 555* (2012) 154–164
DOI: http://dx.doi.org/10.1016/j.matchar.2012.06.013

# Microstructure gradient after hot torsion deformation of powder metallurgical 6061 Al alloy

M. Eddahbi [a,*], A. Borrego [b], M.A. Monge[a], G. González-Doncel [b]

[a] *Department of Physics, Universidad Carlos III, Leganés, 28911 Madrid, Spain*

[b] *Department of Physical Metallurgy, Centro Nacional de Investigaciones Metalúrgicas (CENIM), C.S.I.C., Av. de Gregorio del Amo 8, 28040 Madrid, Spain*

**Abstract:** The microstructure and the texture of extruded 6061 Al alloy processed by powder metallurgy (PM), using three different initial powder particle sizes, have been studied after torsion deformation at 300 °C at strain rate of 6 $s^{-1}$. The initial extruded microstructure of the three alloys consisted of elongated grains confining substructure with a typical ⟨1 1 1⟩+⟨1 0 0⟩ fiber texture. After torsion deformation, the torque ($\Gamma$) as a function of the equivalent strain ($\varepsilon_{eq}$) showed softening and the microstructure exhibited a gradient across the section so that the inner and outer zones contained sheared-elongated and small-equiaxed subgrains, respectively. It was observed that the equivalent strain to failure for the material processed using powder particles size of less than 45 μm was of about $\varepsilon_{eq} \sim 12$, compared to $\varepsilon_{eq} \sim 1$ for material processed using powder particles size of less than 25 μm. The microstructural changes during hot torsion deformation of PM 6061 Al alloy should involve continuous dynamic processes.

**Keywords:** Aluminum alloy Powder metallurgy Torsion deformation Microstructure Recrystallization

## 1. Introduction

Hot working at elevated temperature of aluminum (Al) and Al alloys is of great importance in understanding the materi-als response to deformation conditions and for predicting the microstructural evolution during industrial manufacturing process [1,2]. Hot torsion deformation is used in hot working processes to make it possible to achieve large deformations and grain refinement through the accumulation of strain without the occurrence of plastic instabilities [3]. A complex combination of both restoration and strengthening processes were proposed to explain the microstructural changes at high temperature deformation of Al alloys [4]. It has been reported that Al alloys exhibit very high rates of dynamic recovery rather than dynamic recrystallization, however the formation of new grains during hot deformation has been frequently observed [5]. Different types of dynamic recrystallization, such as discontinuous dynamic recrystallization, continuous dynamic recrystallization, and geometric dynamic recrystallization have been found to occur in Al alloys. In general, highly misoriented subgrains are formed and the misorientation gradually increases during deformation [6].

The 6*xxx* Al alloys series are being widely used as structural material as they show high strength, excellent corrosion resistance, extrudability, and weldability. Specifically, the 6061 Al alloy processed via powder metallurgy (PM) exhibits fine-grained microstructure and better combination of mechanical properties compared to their ingot counterpart. The stability of the final microstructure after hot deformation, i.e. grain size, second phase particles, precipitates and texture, plays a dominant role in controlling the materials properties. The creep behavior and deformation mechanisms of these Al alloys have been extensively studied over a wide range of temperatures at moderate and low strain rates [7,8]. However, the deformation behavior at high temperature and high strain rate has received very limited attention [9,10]. Particularly, in the PM processing, few studies have been concerned with the influence of initial powder particle size on the gradient of microstructure and the properties of processed material by hot tor-sion deformation [11]. Furthermore, the mechanisms controlling the changes in the microstructure after large plastic deformation require further research which would lead to a better understand-ing of the microstructure–properties relationship.

In this study, the changes in the grain structure and texture of extruded 6061 Al alloys processed via PM and subsequent torsion deformation at 300 °C are discussed in the frame of the deformation mechanisms reported for Al alloys [12,13].

## 2. Experimental procedure

The materials used in this study were prepared from 6061 Al alloy powder with the following composition in wt%: 97.74Al–0.96Mg–0.45Si–0.15Fe–0.27Cu [14]. The initial powder was sieved to obtain three different powder particle sizes. Type A

* Corresponding author. Tel.: +34 91 624 6261; fax: +34 91 624 8749.
*E-mail address:* meddahbi@fis.uc3m.es (M. Eddahbi).

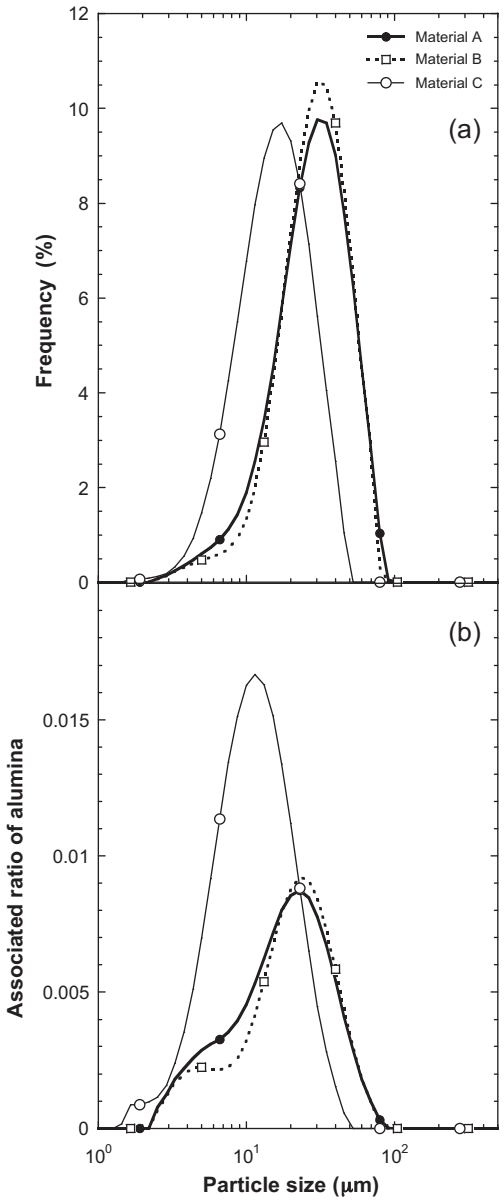


**Fig. 1.** (a) Particle size distribution of materials A, B and C and (b) corresponding volume fraction of alumina.

containing particles size less than 45 μm (not sieved material), type B with powder particles size between 25 and 45 μm (+500 mesh) and type C with powder particles size of less than 25 μm (−500 mesh). Measurements of particle size distribution for each type of powder were performed using powder suspension in ethanol through Mastersizer 2000 applying an impeller speed of 3000 rpm. Five measurements were carried out for each type of powder and the corresponding particle size distributions are shown in Fig. 1(a). Similar particle size distributions were derived from the conventional metallographic method. In this case fifteen images for each type of powder were used. A stereographic method was used to estimate three dimensional particle size distributions from the optical micrographs [15].

Assuming spherical particles of diameter $D$ and an alumina film of thickness $r_o = 4 \times 10^{-3}$ μm covering the particles [6], the ratio of volume of alumina to the volume of the particle was estimated as:

$$\delta = 1 - \left(1 - \frac{2r_o}{D}\right)^3 \quad (1)$$

Evidently, the smaller the powder particle the greater the volume fraction of alumina present as shown in Fig. 1(b).

The materials were processed via a PM procedure in the same way as that described in [16]. All the materials were uniaxially pressed at 400 MPa at a temperature of 100 °C and degassed at about 500 °C for 24 h. The resulting compacts A, B, and C were then extruded at 500 °C at 27:1 reduction, leading to bars of 8 mm in diameter and 1000 mm in length. The same nomenclature as for the sieved powders was kept for the extruded bars. To avoid subsequent precipitation during torsion testing, all materials were over-aged at 300 °C during 24 h.

Samples for torsion tests were machined using a gauge length of 10 mm and a diameter of 5 mm. The torsion tests were carried out at 300 °C at a strain rate of $6\,s^{-1}$. The samples were heated by a high frequency induction furnace in a silica tube in an argon atmosphere. Two-color pyrometers were employed to measure the temperature during the torsion test. At the end of each test the sample was immediately water quenched to retain the deformation microstructure. The torsion test provides the torque ($\Gamma$) versus the number of turns ($N_t$) curves. Then, the equivalent strain ($\varepsilon_{eq}$) and the strain rate ($\dot{\varepsilon}$) were calculated by means of the following relationships [17]:

$$\varepsilon_{eq} = \frac{2\pi R N_t}{L\sqrt{3}} \quad (2)$$

$$\dot{\varepsilon} = \frac{2\pi R \dot{N}_t}{L\sqrt{3}} \quad (3)$$

where $R$ is the sample radius, $\dot{N}_t$ is the number of turns per second and $L$ is the gauge length.

Texture measurements were carried out by means of the Schulz reflection method using a Siemens X-ray diffractometer equipped with a D5000 goniometer. Quantitative three-dimensional orientation distribution functions (ODFs) were obtained using the series expansion method following the Bunge's criterion [18,19]. ODFs were represented with iso-intensity lines at equidistant sections $\Delta\varphi_2 = 5°$ of the Euler's space defined by $\varphi_1$, $\Phi$ and $\varphi_2$ angles.

For metallographical studies, specimens cut from the processed materials and deformed samples were successively grounded and polished and then examined by optical and scanning electron microscopy on a plane parallel to the extrusion axis direction (ED) (or torsion axis). Barker's, Keller's and Poulton's reagents were used to examine the microstructure.

Vickers microhardness measurements were conducted on the longitudinal section of deformed samples to investigate the hardness gradient resulting after torsion deformation. A microhardness test equipment Future-Tech-Corp-Model FM-100e applying a load of 300 g during 25 s was employed for these measurements. The hardness of the original powder was determined by applying a load of 10 g.

## 3. Results and discussion

### 3.1. Initial microstructure

Fig. 2 shows metallographic sections of types A, B, and C powders. Type A powder (no sieved powder) contains the whole range of particle sizes as observed in Fig. 2(a) and (b). The particles are almost spherical, although some of them show irregular shape. Type B powder (+500 mesh) is shown in Fig. 2(c) and (d). It is apparent the presence of particles smaller than 25 μm that have not been completely removed after the sieving process. These particles could have been stuck to other particles that prevent obtaining the expected powder size range. However, the statistical analysis reveals that the amount of particles smaller than 25 μm is about 18% less compared to type A powder. In turn, type C powder (−500

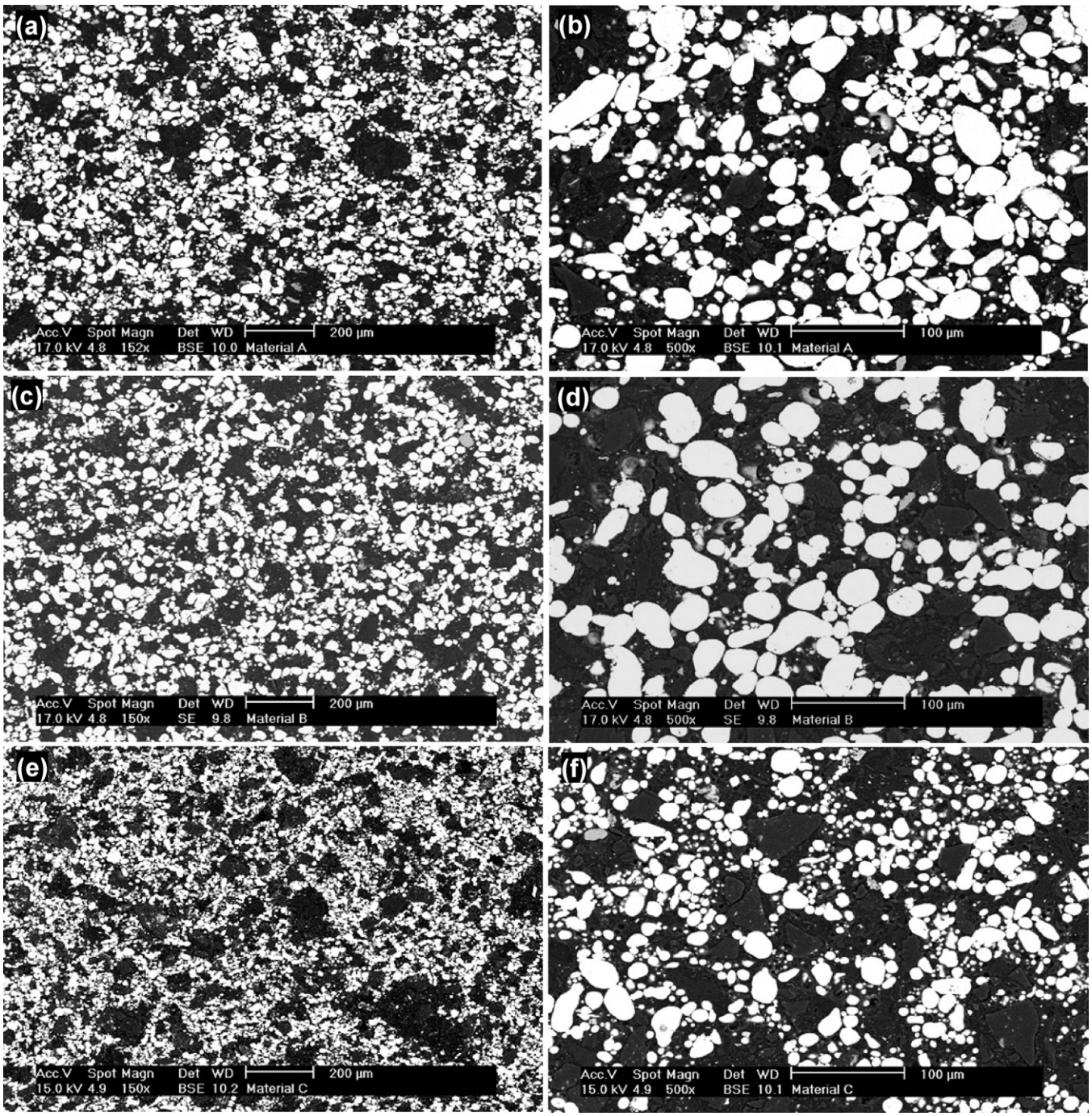


**Fig. 2.** Powder of the 6061 Al alloy: (a) Type A powder (no sieved), (b) high magnification of (a), (c) Type B powder (+500 mesh), (d) high magnification of (c), (e) Type C powder (−500 mesh) and (f) high magnification of (e).

mesh) contains fine particles as shown in Fig. 2(e) and (f). Fig. 3(a) and (b) shows a dendritic structure inside the powder particles, which appears finer in the small ones. The microhardness indentations performed on a large number of particles (Fig. 3(c) and (d)) lead to a hardness of about ∼71 Hv, somewhat higher than the hardness of pure Al (99.6%), ∼23 Hv.

A general view of the microstructure of the extruded PM 6061 Al alloy is shown in Fig. 4. It is important to emphasize that the microstructure of the three materials shows similar characteristics, though the initial particle sizes are different. Fig. 4(a) is a low magnification picture of the microstructure of material A. The original powder particles have undergone plastic deformation during extrusion leading to elongated grains with the long axis parallel to the ED [20]. A uniform banded structure is developed during extrusion, showing a substructure formed at the expenses of a dendritic structure developed inside the elongated grains. Details of the substructure within the elongated grains are visible, as indicated by arrows in Fig. 4(b). Similar observations are made for material B in Fig. 4(c) and (d) and for material C in Fig. 4(e) and (f).

The second phase particles and the precipitates are found inside the grains and at the grain boundaries aligned with the ED [21]. In addition to these particles, a fine dispersion of alumina parti-cles should be present in all materials. These particles result from alumina covering the original powder particles. The amount of alumina is significant in small powder particles, in accordance with

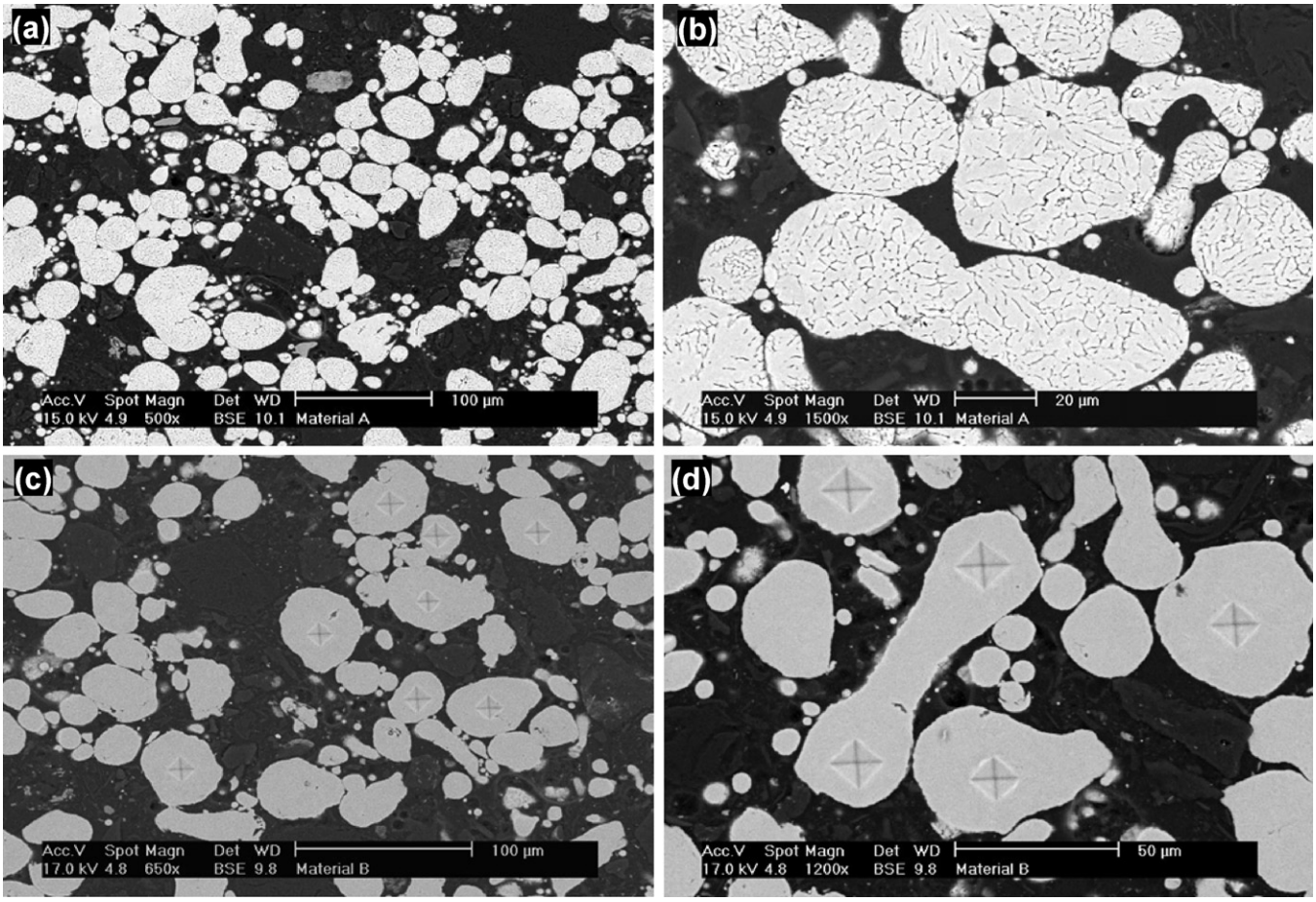


**Fig. 3.** Dendritic structure inside the powder particles: (a) medium magnification and (b) high magnification. Microhardness indentations: (c) medium magnification and (d) high magnification.

Fig. 1(b). Thus, it is expected that material C contains higher amount of alumina particles than materials A and B.

The texture for all materials is described by ⟨1 1 1⟩+⟨1 0 0⟩ fibers, with the fiber axis parallel to ED. The initial deformation texture is more effectively retained in materials A and B than in material C, since material C presents a lower texture intensity ($I = 17.5$) than that of materials A ($I = 29$) and B ($I = 32$).

### 3.2. Torsion tests

The results of the torsion tests for all materials are summarized in the plot of Fig. 5. In this figure, the torque ($\Gamma$) is represented as function of the equivalent strain ($\varepsilon_{eq}$). As is shown, the $\Gamma$ vs. $\varepsilon_{eq}$ curves for materials A and B have a similar peak torque ($\Gamma_p$), but the equivalent strain to failure of material A is twice that of material B, $\varepsilon_{eq} \sim 6$ (which corresponds to number of turns of $N_t \sim 5.8$) against $\varepsilon_{eq} \sim 12$ ($N_t \sim 11.3$). The $\Gamma_p$ for material C is slightly higher whereas the equivalent strain is lower $\varepsilon_{eq} \sim 1$ ($N_t \sim 1$). Two important conclusions can be drawn from Fig. 5, one concerns the softening observed in the $\Gamma$ vs. $\varepsilon_{eq}$ curves and the other is that the $\varepsilon_{eq}$ at $\Gamma_p$ for material C is 3.4 times smaller than the observed value for materials A or B.

The slight increase of $\Gamma_p$ in material C should be related to the initial notable presence of alumina introduced during PM process as illustrated in Fig. 1(b). The interaction of the substructure with the precipitates and oxides can boost strengthening of the material. But, unfortunately, such interaction could also trigger stress concentration, leading to premature failure [22,23]. Similarly, material B may contain enough coarse subgrains (developed from powder size between 25 and 45 μm) whereas material A may contain both coarse and fine subgrains, associated with the whole range of particle sizes of this material (see Fig. 2(a) and (b)). This suggests that the presence of a type C substructure (−500 mesh) in material A may improve the plastic compatibility leading to the observed large plastic flow stability and, therefore, to a high $\varepsilon_{eq}$. In summary, the type C substructure should play a crucial role in accommodating grain fragmentation which is the final microstructural feature for controlling the mechanical characteristics of this material.

### 3.3. Grain structure after torsion deformation

The microstructures of the torsioned materials are shown in Fig. 6(a)–(c) for materials A, B and C, respectively. In all three cases, a microstructural gradient is developed with two distinguishable regions marked as zone 1 and zone 2, which correspond to the outer (surface) and the inner region (centre), respectively. In zone 1, a homogeneous distribution of small equiaxed subgrains less than 1 μm in size is visible. The subgrain at the upper side of the micrographs, close to the grip region, is somewhat coarser than the one in the region near the fracture (bottom side). In zone 2 recrystallization does not take place. The grains are only twisted and become thinner. It is worth noting that the unrecrystallized zone in material C extends from the grip to the fracture region, Fig. 6(c), whereas in material A it becomes less apparent toward the fracture region, Fig. 6(a). Furthermore, shearing in zone 2 of material A seems to be progressive, according to the angle between the long

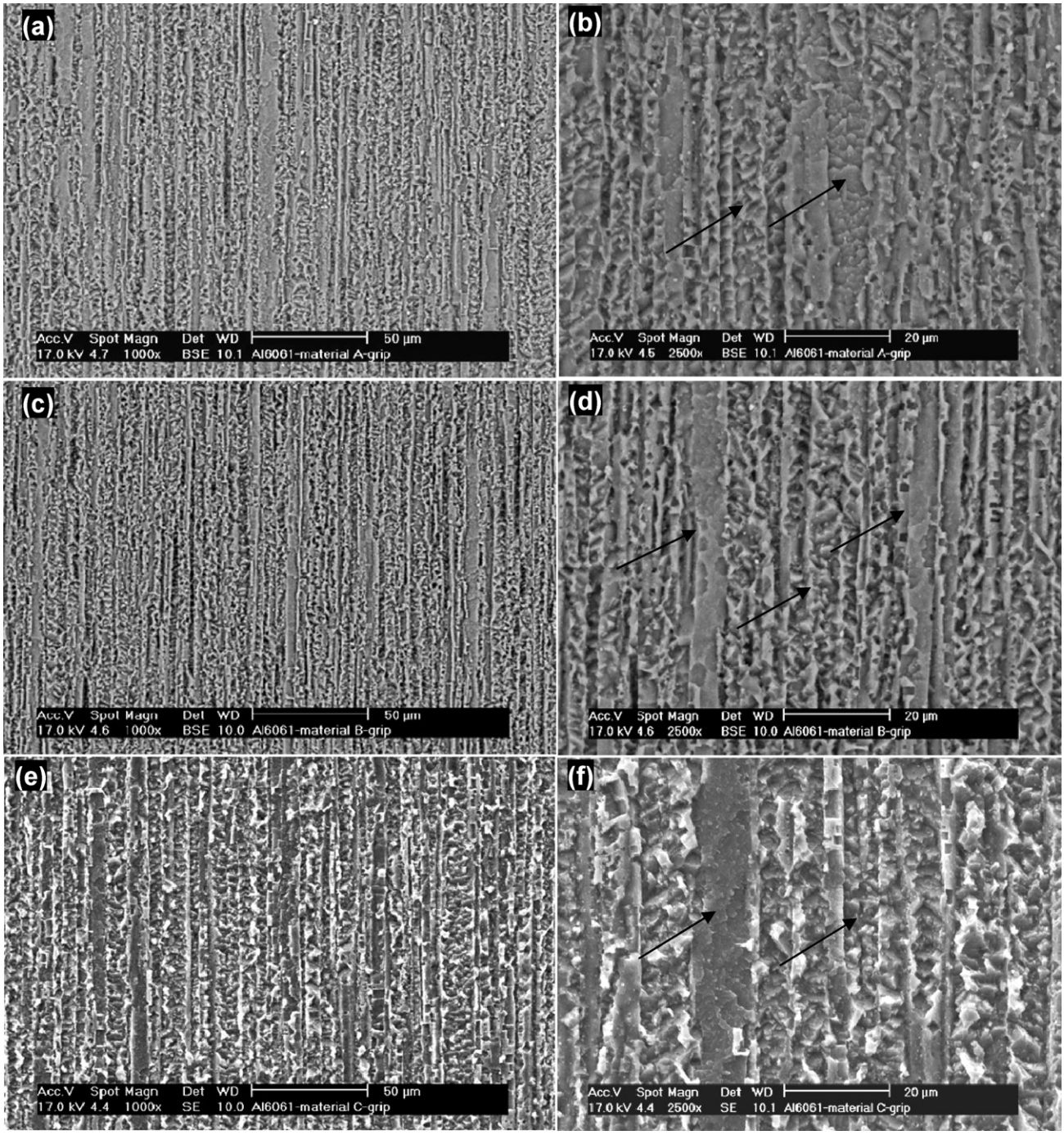


**Fig. 4.** (a) Microstructure of material A showing elongated banded structure parallel to ED, (b) high magnification of (a). Similar banded microstructure is also apparent for material B: (c) low magnification, (d) high magnification of (c) and for material C: (e) low magnification and (f) high magnification of (e). The arrows indicate the substructure inside the banded structure.

axis of deformed grains and the torsion axis. This angle is low at the proximity of the grip region but it increases along the gauge, reaching the maximum value at the fracture region. This indicates the increasingly deformed microstructure and shearing change with the fragmentation process through zone 2. This results in a more effective refinement of the microstructure. These effects are clearly revealed in material A where the angle in the grip region is of about 45° and increases to 90° near the fracture. The microstructure gradient developed in PM 6061 Al alloy is commonly observed in materials deformed in torsion, which is associated with inhomogeneous deformation or strain rate through the radius, maximum at the surface and minimum at the centre [24].

The evolution of the deformed grain structure is also observed from the change in the alignment of the second phase particles as shown in Fig. 7. This figure illustrates the alignment of these particles on a longitudinal plane of materials B and C. In the grip regions the particles are aligned with the ED, as observed in Fig. 7(a) and (d). However, in the deformed regions the particles alignment changes dramatically from zone 2 to zone 1. In zone 2, the second phase particles reorient as shown in Fig. 7(b) and (e). In contrast, such alignment is broken up in zone 1 by shear deformation, and the particles become uniformly distributed in the matrix, Fig. 7(c) and (f). Similar changes in the alignment of particles in zone 1 and 2 are also found in material A.

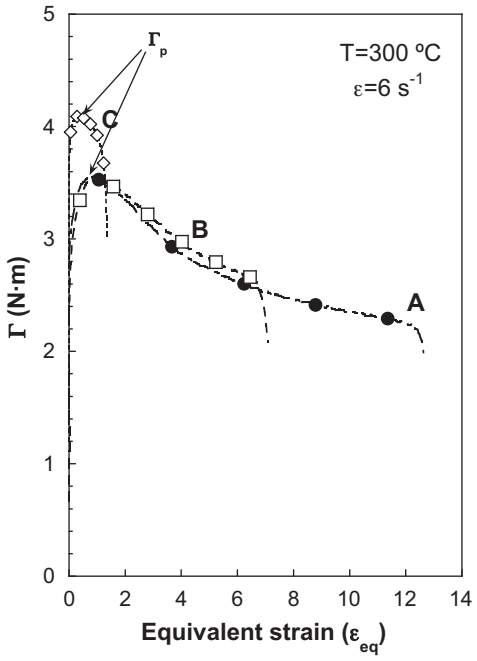


**Fig. 5.** Torque as function of equivalent strain curves of materials A, B and C.

### 3.4. Microhardness measurements

Fig. 8 shows the hardness along ED in zone 2 of deformed materi-als. It can be seen that the hardness along the torsion axis increases from the grip to the fracture region. This is consistent with the deformation gradient observed along this direction. The hardness along the diameters $d_1$, $d_2$ and $d_3$ of deformed samples are shown in Fig. 9(a)–(c) for materials A, B and C, respectively. For compari-son, the hardness at the grip regions and the hardness of the 6061 Al powder particles are also included. As observed, the powder has higher hardness than any of the three materials. This is due to the high amount of atoms in solid solution in the dendritic structure. Furthermore, it is remarkable that the material C reveals a low hard-ness in spite of its high content of alumina particles (see Fig. 1(b)). This material, however, has the lowest texture intensity of all three materials [25]. Then, their difference in hardness should be due to the texture rather than to the presence of the oxides. However, under torsion deformation at 300 ◦C the thermally activated pro-cesses become more important and, thus, the strengthening due to oxide-dislocation interactions should be more pronounced in material C than in materials A and B, as revealed by the increase of $\Gamma_p$ in the $\Gamma$ vs. $\varepsilon_{eq}$ curves.

An important consideration arising from Fig. 9 is the hardness decrease from the outer region towards the inner region of the torsioned samples. This variation in hardness across the radius is noticeably more marked for material C ($N_t \sim 1$) than for material A ($N_t \sim 11.3$), compare Fig. 9(a) and (c). It is related to the gradient of

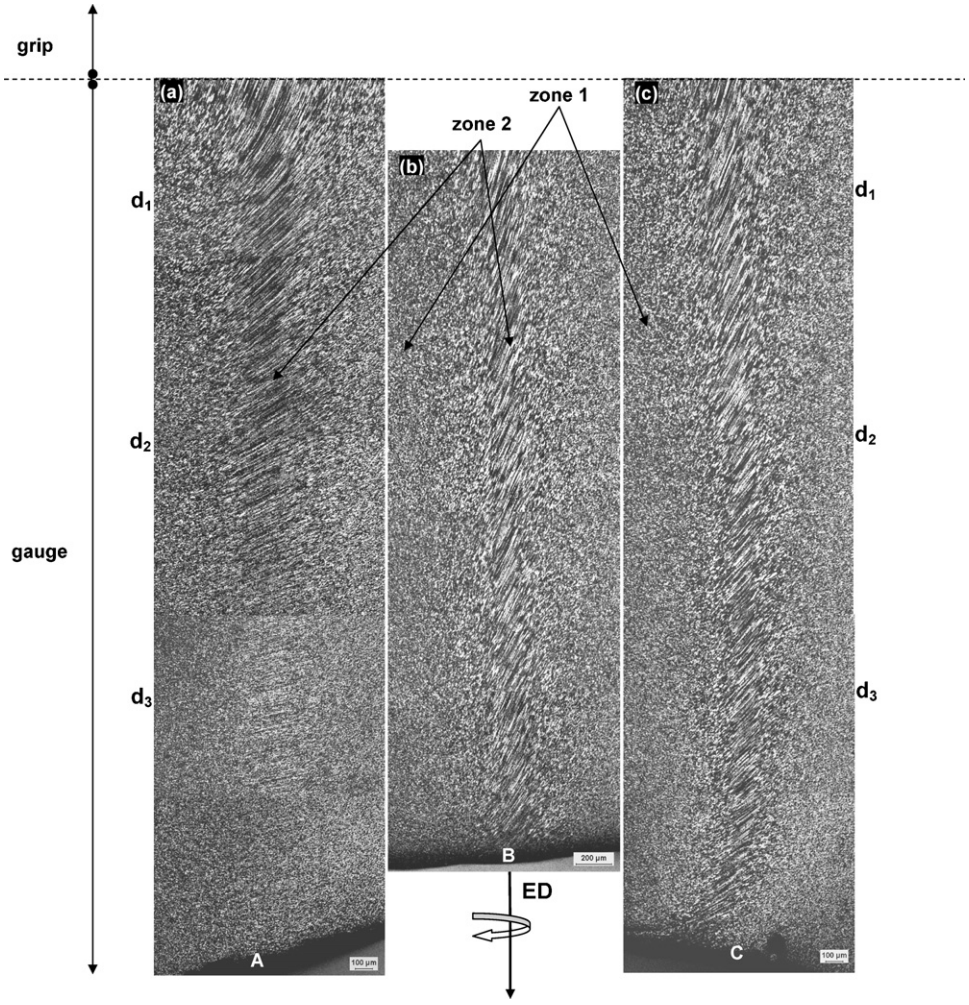


**Fig. 6.** Deformed microstructures (longitudinal section) in the gauge region of: (a) material A, (b) material B, and (c) material C.

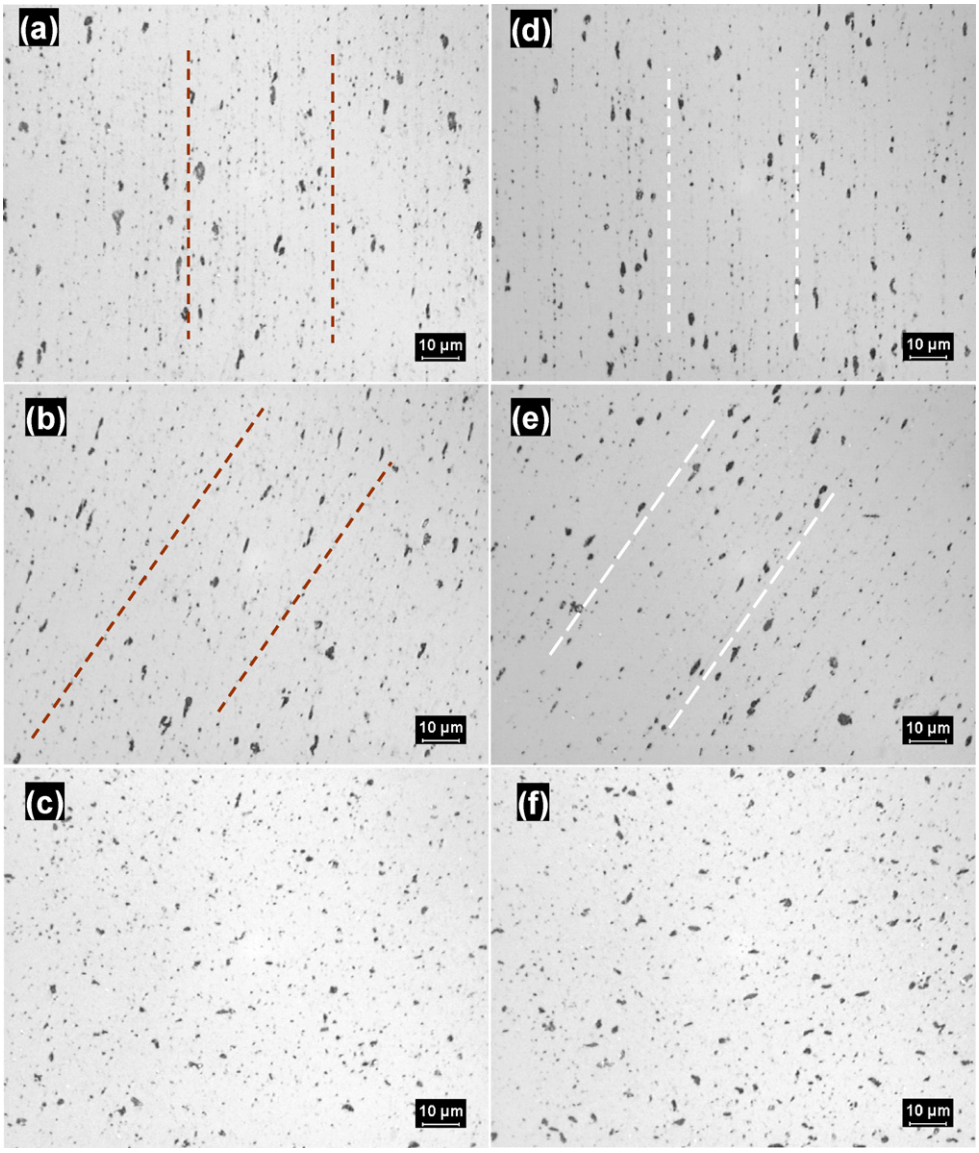


**Fig. 7.** Alignment of second phase particles after torsion deformation (longitudinal section): (a)–(c) correspond to: grip region, zone 2, and zone 1, respectively, of material B and (d)–(f) correspond to the same regions of material C.

the microstructure shown in Figs. 6 and 7; i.e. the grain refinement increases from grip towards the fracture region and decreases from the surface towards the centre of the strained samples. Similar changes in hardness across the radius of deformed sample were observed in a series of Al alloys processed by high pressure torsion (HPT), as for example pure Al, 6061 Al alloy, and strengthened Al–Mg alloy [26–29]. Then, there is clear evidence for evolution towards a more homogeneous microstructure with increasing equivalent strain (or $N_t$).

If the average hardness at $d_i$ ($1 \leq i \leq 3$) of materials A, B and C is plotted as a function of the corresponding equivalent strain (or as a function of the number of turns $N_t$) then the data will lie on a single curve, which should be described by three main stages, I, II and III, as shown in Fig. 10. In stage I the hardness increases until reaching a maximum located at $\varepsilon_{eq}$ between ~1 and ~6 (extrapolated point) and then decreases in stage II with a further strain up to 12. A very large strain is expected in stage III, where the hardness should be constant. This hardness variation with $\varepsilon_{eq}$ at room temperature of PM 6061 Al alloy is in good agreement with the softening observed in $\Gamma$ vs. $\varepsilon_{eq}$ curves in Fig. 5. On the basis of this representation, it is reasonable accepting that the hardness of sample C belongs to stage I (strengthening), where the recrystallized microstructure is low compared to materials A and B, which belong to stage II (softening). The microstructure in stages II and III should be characterized by a progressive increase in the recrystallized microstructure and then an equilibrium grain structure should be achieved. It is proposed that the strengthening and softening of PM 6061 Al alloy during torsion deformation is controlled by the fragmentation process, depending on the change in the recrystallized volume.

The evolution of hardness with the number of turns during HPT has been studied in numerous materials, and different views have been proposed to determine the softening mechanism [30–32]. It was suggested that the average size of grains with highly misoriented boundaries is the important parameter influencing the softening and strengthening during the HPT process [32]. Also, the higher the homologous temperature, $T_H$ ($T_H = T/T_m$ where $T$ is the temperature test and $T_m$ is the melting temperature), and/or the stacking fault energy, the more predominant the dynamic softening processes. On the contrary, the PM 6061 Al alloy treated in this study exhibits softening even though it was reported that the stacking fault energy is lower than that of pure Al [34]. However, softening and hardening have been observed in 6061 Al alloy under

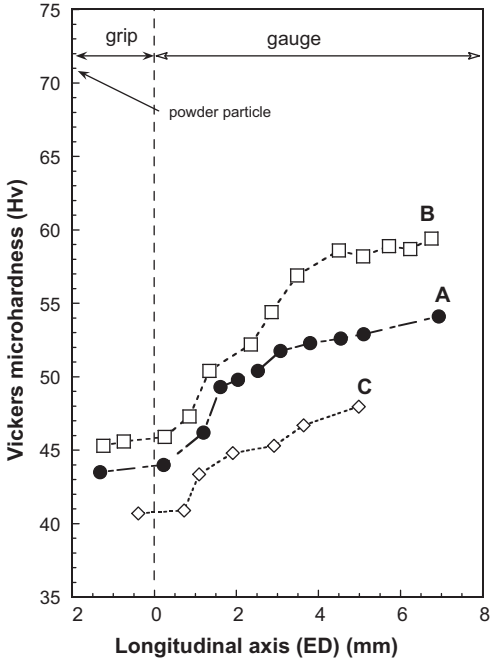


**Fig. 8.** Microhardness profiles in zone 2 along the torsion axis ED of the three samples.

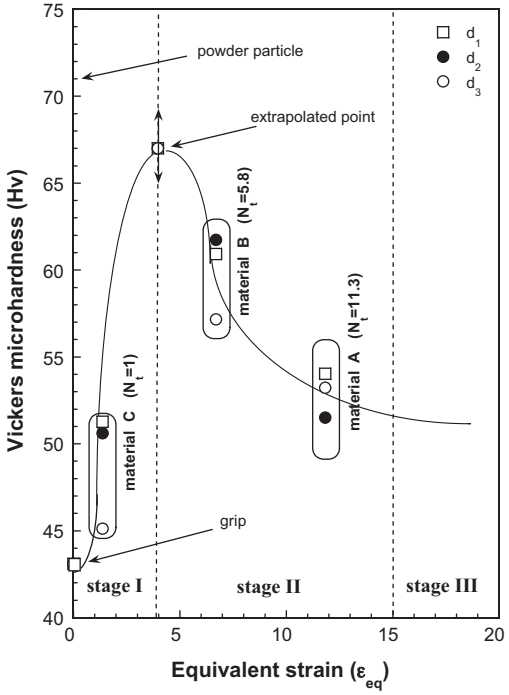


**Fig. 10.** Average microhardness values across $d_1$, $d_2$, and $d_3$ as a function of equivalent strain of materials A, B, and C.

torsion deformation at high homologous temperatures of $T_H = 0.72$ and 0.81 [24] and under HPT and ECAP at $T_H = 0.32$ [33,34] whereas the grain size increases with increasing $T_H$. Further studies are, hence, needed to understand the microstructural changes involved during torsion deformation and the relationship between softening processes and $T_H$.

### 3.5. Texture after torsion deformation

Fig. 11 represents the ODFs through $\varphi_2$-sections and the spa-tial arrangement of the fibers in the Euler's space of materials A (Fig. 11(b)), B (Fig. 11(c)) and C (Fig. 11(d)) after torsion deforma-tion. It is important to note that the texture measurements were carried out on the longitudinal plane of deformed samples, including zone 1 and zone 2. For comparison, the ODFs and Euler's space evaluated in the grip region of sample C are also introduced in Fig. 11(a). This texture should be considered as the initial one for all torsion tests since the pre-annealing treatment does not affect the microstructure. It can be described by a set of orientations starting at $(0\,1\,1)[1\,\bar{1}\,1]$ and extending from $(1\,1\,0)[1\,\bar{1}\,1]$ to $(1\,0\,1)[\bar{1}\,\bar{1}\,1]$, i.e. $\langle 1\,1\,1\rangle$ fiber orientations. After torsion deformation, this fiber is found in the gauge region of all the deformed materials. However, its intensity decays. This texture appears similar to the one obtained in pure Al deformed in torsion up to 31 equivalent strain at 400 °C, at strain rate of $5 \times 10^{-2}$ s$^{-1}$ and in 1050 Al alloy deformed in torsion

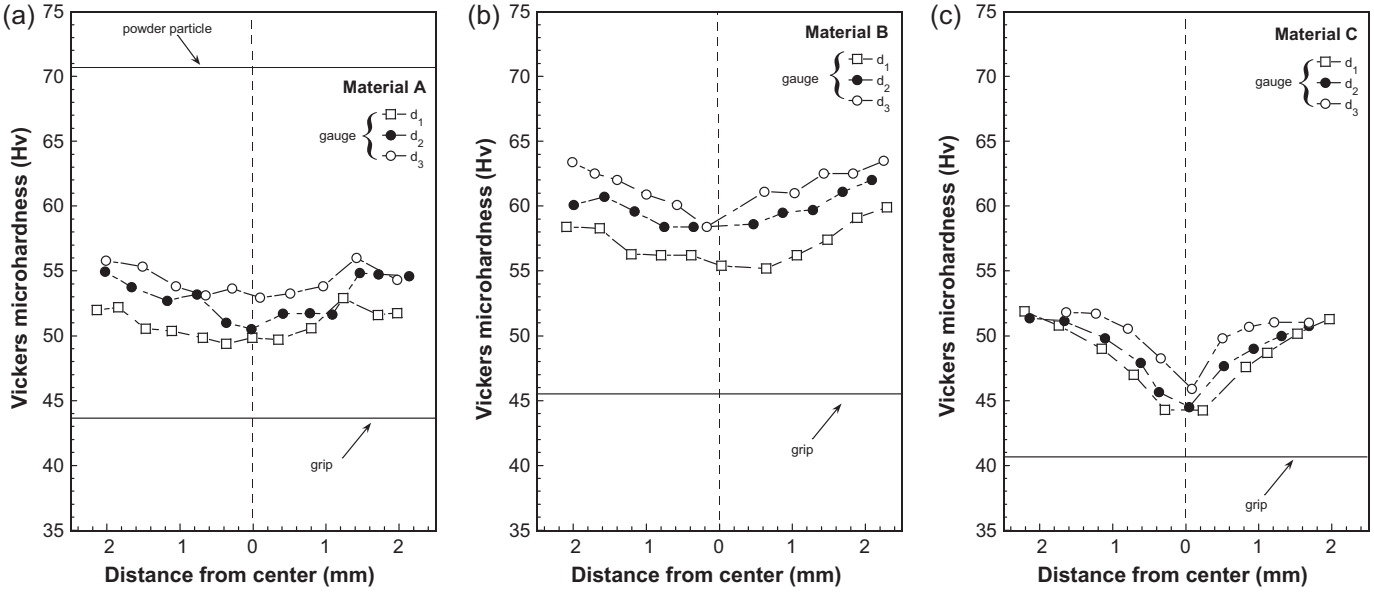


**Fig. 9.** Microhardness profiles across diameters denoted as $d_1$, $d_2$, and $d_3$ in Fig. 6 of (a) material A, (b) material B, and (c) material C.

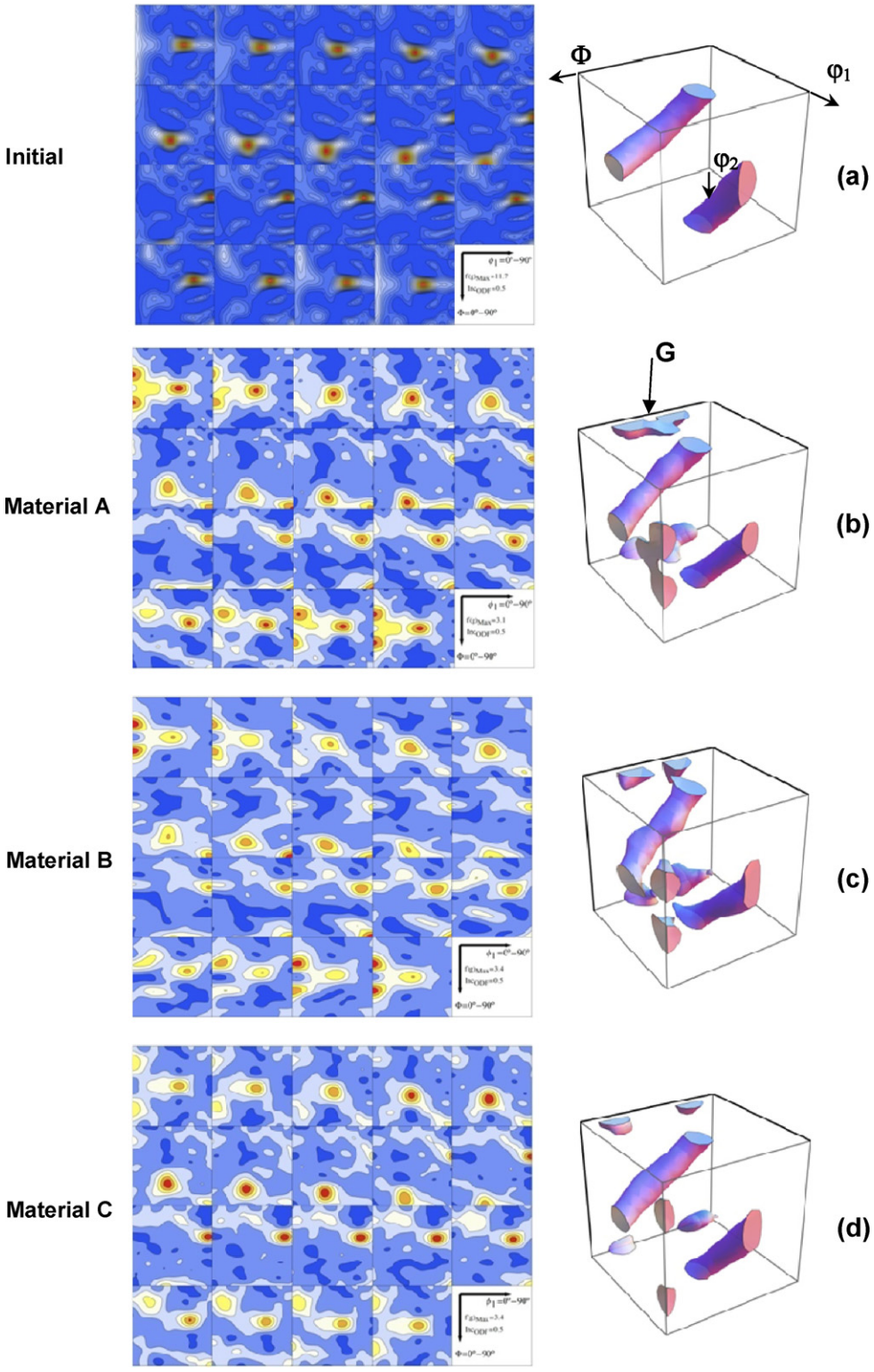


**Fig. 11.** Texture represented as ODFs sections ($\varphi_2$ = cte) and spatial arrangement of the fibers in the Euler's space: (a) initial, and gauge region of (b) material A, (c) material B and (d) material C.

at a strain of 7 at 450 °C at strain rate of 0.1 $s^{-1}$ [35,6]. A similar result was also found in Al strained by HPT at room temperature [36]. Furthermore, for $\varphi_2 = 0°$ it can be seen the emergence of (0 1 2)[1 0 0] orientation for samples A and B and the (0 1 3)[1 0 0] orientation for sample C, Fig. 11(b)–(d), respectively. These orientations are related to a rotation about ⟨1 0 0⟩. Therefore, the cube orientation {1 0 0}⟨1 0 0⟩ evolves towards the Goss orientation, {1 1 0}⟨1 0 0⟩ (G), during torsion deformation.

The intensity of the global texture after torsion deformation is low ($I \sim 3$), compared to the initial one, despite the difference observed for the equivalent strain to failure. For example, the texture intensity in sample C decreases dramatically, from $I \sim 17$ to

close to $I \sim 3$ in a short strain interval of about ~1, while sample A exhibits large equivalent strain to failure, $\varepsilon_{eq} \sim 12$, and the final texture intensity approaches 3. This means that (i) the premature failure of sample C is not caused by texture softening, and (ii) the texture decrease, as well as most microstructural changes should occur in a strain interval below 2. On the other hand, it is observed that the fibers orientations persist in zone 1 even after a large strain is achieved. This indicates that the fragmentation of the microstructure does not randomize the texture in the recrystallized regions, i.e. a fraction of subgrains which accommodate the deformation with respect to their neighbors should maintain their orientation.

### 3.6. Hot deformation behavior

In accordance with the microstructure developed after torsion tests (Fig. 6), it seems that the softening observed in $\Gamma$ vs. $\varepsilon_{eq}$ curves (Fig. 5) cannot be explained in terms of discontinuous or geomet-ric dynamic recrystallization. This is because neither signal of grain boundary migration nor serrated grain boundaries are observed in the deformed microstructures [37–41]. Moreover, deformation shear bands associated with adiabatic heating are not observed under the testing conditions of this study, which generally should produce softening [42]. It is the initial banded structure which frag-ments during torsion deformation, assisted by continuous dynamic processes. During early stages of deformation, up to a strain of less than ~2 (stage I in Fig. 10), the texture vanishes and small subgrains develop, especially at the outer region of the deformed samples. Since materials A and B develop similar end texture, whereas $\varepsilon_{eq}$ differs by a factor of two, it is expected that the texture remains constant in the progress of shearing beyond $\Gamma_p$ (stage II in Fig. 10).

There is lack of data about the texture of PM Al alloys after torsion deformation, whereas texture of cast Al and Al alloys after hot working has been reported [3,35]. It was observed that the texture often becomes weak after large torsion deformation, similar to that observed in the PM 6061 Al alloy of this study, and in 6061 Al alloy processed by ECAP [34,43]. Furthermore, the effect of rotation of cube orientation on softening is insignificant, although the Taylor's factor due to the evolution of texture during torsion can decrease [44,45]. This effect can contribute only partially to the softening [46,47]. As anticipated in Section 3.5, we can conclude, therefore, that softening of PM 6061 Al alloy cannot be due to the texture.

On the other hand, neither dynamic subgrain growth nor agglomeration of second phase particles is observed in PM 6061 Al alloy after torsion. Both can also promote softening [34]. The microstructure in the recrystallized regions may remain constant in the softening stage beyond $\Gamma_p$ (stage II in Fig. 10). This is supported by the fact that the subgrain size of material C in the recrystallized region is similar to that of materials A and B. However, if the material A, supposedly, had the capacity to deform above a strain of 12, then the microstructure could have been totally recrystallized in stage III, and no sheared zone 2 would be apparent. This result is consistent with that obtained in Al and Al alloys after large torsion deformation [3]. Under these conditions, an equilibrium grain structure independent of the initial grain size is developed [24,48]. The same tendency was observed in materials processed by ECAP and HPT. For example, small grains of about 0.9 and 1.2 μm were developed in Al–Li and Al–Cu alloys deformed by ECAP up to strain 12 via route A at 300 and 250 °C, respectively [49,50]. Also, ultrafine grains of 0.25 μm in size were developed under HPT after 20 turns at room temperature [33].

There is an agreement that the grain fragmentation in Al and Al alloys processed by different thermomechanical routes, such as torsion, compression, ECAP, or HPT is usually accompanied by a decrease of the initial texture, and an increase of the average misorientation between neighbors; low angle boundaries gradually transform into high angle boundaries [49,50,41]. Nevertheless, there is a difference in the strain conditions for the onset of the formation of the new substructure, at least under torsion deformation conditions. For example, it has been reported in several studies that the substructure develops during the early stages of deformation up to the peak stress [6,51,52]. By contrast, it has been concluded in an early study that subgrain boundaries in Al do not form until $\Gamma_p$ is reached [38,53]. Furthermore, new subgrains were not developed in a 6061 Al alloy until certain strain beyond the peak stress was attained [24]. Grain rotation, grain boundary sliding and diffusion creep can also operate during torsion deformation that would hide the main deformation mechanism responsible for softening. More microscopic observations and mechanical tests are needed to deepen our knowledge of the correlation between softening, grain structure, texture–microtexture, and homologous temperature during hot torsion deformation.

## 4. Conclusions

The microstructure and the texture of three extruded 6061 Al alloys processed by powder metallurgy route using different particle sizes have been studied after torsion deformation at 300 °C at strain rate of $6\,s^{-1}$. The main findings of this study are as follows:

1. The extruded 6061 Al alloys showed a banded structure, consisting of elongated grains confining a fine substructure. The texture was described by ⟨1 1 1⟩+⟨1 0 0⟩ fibers, typical of extruded Al alloys.
2. The torsioned samples developed a gradient of microstructure through the diameter: the inner zone contained sheared grains and the outer zone contained new small recrystallized subgrains inferior to 1 μm, formed by the fragmentation of the original grains. The initial texture intensity decreased dramatically.
3. The $\Gamma$ vs. $\varepsilon_{eq}$ curves of all deformed materials reveal softening. The alloy processed from powder particle of less than 45 μm in size showed $\varepsilon_{eq} \sim 12$, whereas the alloy processed form powder particles of less than 25 μm in size showed $\varepsilon_{eq} \sim 1$. This result was associated with the fragmentation of the banded structure assisted by a continuous dynamic process.

## Acknowledgments

The authors thank CM (program TECHNOFUSION-CM S2009/ENE-1679) and CM/UE: Project MATERA/ESM-1889 and Spanish Ministry of Science and Innovation: Project MAT09-09545. Thanks are also due to Dr. Carsí for his help with the torsion tests.

## References

[1] J.J. Jonas, C.M. Sellars, W.J.McG. Tegart, Metall. Rev. 130 (1969) 1–24.
[2] F. Bardi, M. Cabibbo, E. Evangelista, S. Spigarelli, M. Vukčevič, Mater. Sci. Eng. A39 (2003) 43–52.
[3] M.E. Kassner, M.M. Myshlyaev, H.J. McQueen, Mater. Sci. Eng. A108 (1989) 45–61.
[4] H.J. McQueen, Mater. Sci. Eng. A387–A389 (2004) 203–208.
[5] R.D. Doherty, D.A. Hughes, F.J. Humphreys, J.J. Jonas, D. Juul Jensen, M.E. Kassner, W.E. King, T.R. McNelley, H.J. McQueen, A.D. Rollett, Mater. Sci. Eng. A238 (1997) 219–274.
[6] M.R. Barnett, F. Montheillet, Acta Mater. 50 (2002) 2285–2296.
[7] R. Fernández, G. González-Doncel, J. Alloys Compd. 440 (2007) 158–167.
[8] K.T. Park, E.J. Lavernia, F.A. Farghalli, Acta Metall. 42 (1994) 667–678.
[9] J.R. Pickens, T.J. Langan, R.O. England, M. Liebson, Metall. Mater. Trans. A 18 (1987) 303–312.
[10] Si.Y. Chang, Ki.S. Lee, S.-H. Choi, D.H. Shin, J. Alloys Compd. 354 (2003) 216–220.
[11] S.J. Hong, B.S. Chun, Mater. Sci. Eng. A348 (2003) 262–270.
[12] L.M. Dougherty, I.M. Robertson, J.S. Vetrano, Acta Mater. 51 (2003) 4367–4378.
[13] F.J. Humphreys, M. Hatherly, Recrystallization, Related Annealing Phenomena, 2nd ed., Pergamon, 2004.
[14] A. Borrego, Ph.D. dissertation, Universidad Complutense de Madrid, 2003.
[15] Y-H. Xu, H.C. Pitot, Comput. Methods Programs Biomed. 72 (2003) 1–20.
[16] M. Eddahbi, Ph.D. dissertation, Universidad Complutense de Madrid, 1998.

[17] M. Carsí, V. Lódpez, F. Peñalba, O.A. Ruano, Mater. Sci. Eng. A216 (1996) 155–160.
[18] H.J. Bunge, Texture Analysis in Materials Science, 2nd ed., Butterworths, London, 1982.
[19] V. Randle, O. Engler, Texture Analysis, Macrotexture, Microtexture and Orientation Mapping, Gordon and Breach, London, 2000.
[20] M. Bauser, G. Sauer, K. Siegert (Eds.), Extrusion, ASM International, The Materials Information Society, Materials Park, Ohio, 2006.
[21] H.J. McQueen, O.C. Celliers, Can. Metall. Q. 35 (1996) 305–319.
[22] M. Eddahbi, F. Carreño, O.A. Ruano, Mater. Lett. 60 (2006) 3232–3237.
[23] M. Eddahbi, J.A. Jiménez, O.A. Ruano, J. Alloys Compd. 433 (2007) 97–107.
[24] W.H. Van Geertruyden, Z.W. Misiolek, P.T. Wang, Mater. Sci. Eng. A419 (2006) 105–114.
[25] R. Bauri, V. Pancholi, I. Samajdar, M.K. Surappa, Sci. Tech. Adv. Mater. 6 (2005) 933–938.
[26] C. Xu, Z. Horita, T.G. Langdon, Acta Mater. 56 (2008) 5168–5176.
[27] A.P. Zhilyaev, K. Oh-ishi, T.G. Langdon, T.R. McNelley, Mater. Sci. Eng. A410–A411 (2005) 277–280.
[28] J. Zhang, M.J. Starink, N. Gao, W. Zhou, Mater. Sci. Eng. A528 (2011) 2093–2099.
[29] G. Sakai, K. Nakamura, Z. Horita, T.G. Langdon, Mater. Sci. Eng. A406 (2005) 268–273.
[30] Y. Ito, Z. Horita, Mater. Sci. Eng. A503 (2009) 32–36.
[31] K. Edalati, Z. Horita, Mater. Sci. Eng. A528 (2011) 7514–7523.
[32] K. Edalati, Z. Horita, Acta Mater. 59 (2011) 6831–6936.
[33] A. Loucif, R.B. Figueiredo, T. Baudin, F. Brisset, R. Chemam, T.G. Langdon, Mater. Sci. Eng. A532 (2012) 139–145.
[34] C. Xu, M. Furukawa, Z. Horita, T.G. Langdon, Mater. Sci. Eng. A398 (2005) 66–76.
[35] F. Montheillet, M. Cohen, J.J. Jonas, Acta Metall. 32 (1984) 2077–2089.
[36] D. Orlov, P.P. Bhattacharjee, Y. Todaka, M. Umemoto, N. Tsuji, Scr. Mater. 60 (2009) 893–896.
[37] T. Sakai, M.G. Akbeny, J.J. Jonas, Acta Metall. 31 (1983) 631–642.
[38] M.J. Luton, C.M. Sellars, Acta Metall. 17 (1969) 1033–1043.
[39] H.J. McQueen, Q. Knustard, N. Ryum, Scr. Mater. 19 (1995) 73–78.
[40] G.A. Henshall, M.E. Kassner, H.J. McQueen, Metall. Mater. Trans. A 23 (1992) 881.
[41] W. Blum, Q. Zhu, R. Merkel, H.J. McQueen, Mater. Sci. Eng. A205 (1996) 23–30.
[42] G.M. Owolabi, A.G. Odeshi, M.N.K. Singh, M.N. Bassim, Mater. Sci. Eng. A457 (2007) 114–119.
[43] Q. Jining, J.H. Han, Z. Guoding, J.C. Lee, Scr. Mater. 51 (2004) 185–189.
[44] G.A. Henshall, M.E. Cáncer, H.J. McQueen, Metall. Mater. Trans. A 23 (1992) 881–889.
[45] C. Perdrix, M.Y. Perrin, F. Montheillet, Mem. Sci. Rev. Met. 78 (1981) 309–320.
[46] J.K. Solberg, H.J. McQueen, N. Ryum, E. Nes, Philos. Mag. 4 (1989) 447–471.
[47] H.J. McQueen, J.K. Solberg, N. Ryum, E. Nes, Philos. Mag. 4 (1989) 473–485.
[48] H.J. McQueen, O. Knustad, N. Ryum, J.K. Solberg, Scr. Mater. 19 (1985) 73–78.
[49] R. Kaibyshev, K. Shipilova, F. Musin, Y. Motohashi, Mater. Sci. Eng. A396 (2005) 341–351.
[50] I. Mazurina, T. Sakai, H. Miura, O. Sitdikov, R. Kaibyshev, Mater. Sci. Eng. A486 (2008) 662–671.
[51] I. Gutiérrez, F. Castro, J.J. Urcola, M. Fuentes, Z. Metallkd. 81 (1990) 136–143.
[52] D. Hardwick, W.J.McG. Tegart, J. Inst. Met. 90 (1961) 17–21.
[53] V.A. Lekhachev, M.M. Myshlyaev, O.N. Senkov, S.P. Belyayev, Phys. Met. Metallogr. 52 (1981) 156.